Available online at www.sciencedirect.com
ScienceDirect
Physics Procedia 56 (2014) 582 – 590
Physics Procedia

8th International Conference on Photonic Technologies LANE 2014

Laser beam welding of thick titanium sheets in the field of marine technology

André Schneider[a,*], Andrey Gumenyuk[a], Marco Lammers[a], Andreas Malletschek[b], Michael Rethmeier[a]

[a]*BAM - Federal Institute for Materials Research and Testing, Germany*
[b]*ThyssenKrupp Marine Systems GmbH, Germany*

Abstract

The ever larger requirements of the material selection in the range of maritime industry necessitate the application of high-tech materials. Titanium because of its excellent mechanical properties at low weight is an attractive alternative for the construction of ships. The goal of this investigation was to design a welding method for joining samples of 16 mm thick Ti3Al2.5V. The welding experiments with a 20 kW Yb-fiber laser source and varying combinations of parameters were intended to qualify the laser beam welding process. The welding results were analyzed by non-destructive and destructive testing. In addition, the welding tests were recorded with two high-speed cameras to observe the weld pool and the vapor plume. The evaluation of the high-speed images in correlation with the results of non-destructive testing shows, that a significant improvement of process stability and weld quality can be achieved by the suppression of the vapor plume.

Peer-review under responsibility of the Bayerisches Laserzentrum GmbH
Keywords: titanium alloy; maritime industry; vapor plume; laser beam welding; Ti3Al2.5V

1. Motivation

Military and civilian shipbuilding requirements for materials selection and technical design of seagoing vessels and their components are growing (Malletschek (2011)). The tolerable load needs to be increased despite of the reduction in overall weight. Furthermore, the service life of the finished components needs to be prolonged, which goes hand in hand with a reduced susceptibility to corrosion. As an alternative to traditional materials like steel, titanium and its alloys are available, for example. Titanium has about half the density and similar strength compared to conventional shipbuilding steels (Boyer et al. (2007); Peters and Leyens (2002)). Thanks to its exceptionally good corrosion resistance, titanium, although more costly, represents an alternative to the previously used steel. In offshore applications, titanium alloys are very widespread being no longer an exception (Caplan (1986)). Offshore platforms strained by seawater provide good conditions for the use of titanium alloys. In marine research titanium is frequently used. The high technical requirements for measuring and working equipment in marine research make titanium an

* Corresponding author. Tel.: +49-30-8104-3101 ; fax: +49-30-8104-1557 .
E-mail address: andre.schneider@bam.de

Peer-review under responsibility of the Bayerisches Laserzentrum GmbH
doi:10.1016/j.phpro.2014.08.046

obvious choice for its application as an ideal construction material. Military shipbuilding has begun to use titanium alloys for seagoing vessels and submarines (Malletschek (2011)). The plate thicknesses used here are in the double digit millimeter range. Joining of these thicknesses is a major challenge to the welding technique used. Here, laser beam welding has shown itself to be particularly suitable. Due to the high energy input respectable penetration depths can be achieved. The subject matter of the investigations was the development of suitable welding parameters for joining Ti3Al2.5V samples with a thickness of 16 mm.

2. State of the Art

In deep penetration high-power solid state laser beam welding of metals, the welding plume consists of two different parts. They differ in temperature, brightness and their geometrical form, respectively. The lower part (referred to as welding plasma) shows a sharp boundary with a height of up to 5 mm and a maximum temperature of 4500 K. The upper part of the welding plume can reach up to 50 mm in height with a constant temperature of 2000 K (Shcheglov (2012)). In this area, the brightness is decreasing and there are no sharp boundaries apparent. The vapor is only weakly ionized and a metal vapor cloud is formed instead of the plasma. The diameter of particles in this cloud are between 10 nm and 100 nm (Anisimov (1967)). Through these particles a part of the laser beam is scattered and thus attenuate its power (Shcheglov et al. (2011)). Furthermore it comes to a refraction of the laser beam by the density gradient between the ambient air and the plume. A convex temperature distribution determines a concave density distribution. Both mentioned effects result in a strong defocusing of the laser radiation causings a variation of the power density in the laser beam and the molten metal interaction zone. Penetration depth is reduced as a result of the evolving plume caused by the escape of metal vapor from the keyhole and its recondensation above the workpiece surface (Hügel and Dausinger (2004)). The transmitted fraction of laser radiation in the plume decreases with growing plume size. Inside the keyhole the laser beam absorption is characterized by two main effects, i.e. inverse Bremsstrahlung and Fresnel absorption (Yi et al. (2005); Tu et al. (2003)). The plume above the workpiece surface permits less laser power to penetrate into the keyhole and thus reduces these two effects described. A suitable inert gas shield may suppress the plume and thus allow more laser beam power to be introduced into the keyhole. A shielding gas nozzle laterally aligned to the weld has a direct influence on plume formation (Li et al. (2010)). The high affinity of titanium to the atmospheric gases oxygen, nitrogen and hydrogen calls for an additional gas shield of the weld during cooling. Titanium dissolvability for these gases clearly starts at a temperature of 400 °C (DVS2713 (2003)) and reaches a minimum value at 300 °C (Bungardt and Rüdinger (1956)). The oxygen content of the ambient air during welding can be concluded based on the temper colors of the weld (Bergmann (2004)). Material hardening occurs with increasing oxygen content (Li et al. (2005)).

3. The influence of the vapor plume

A 20 kW Yb fiber laser source (YLR-20000, IPG Photonics) with a fiber diameter of 200 µm was used in the experiments. The beam parameter product of the laser corresponds to 11.5 mm·mrad. The applied welding optics has a focusing module with 350 mm focal length and a collimator of 125 mm. The resulting magnification of 2.3 corresponds to a theoretical focal spot diameter of 560 µm, at a Rayleigh length of 5.7 mm. The samples of alloy Ti3Al2.5V had a thickness of 16 mm and dimensions of 350 mm × 40 mm. Each set consisted of one pair which was butt welded, see Figure 1. The composition of the samples is listed in Table 1 as specified by the manufacturer.

Table 1. Composition of Ti3Al2.5V in %.

Al	V	O	Fe	Cr	N	C	H	residual each	residual total	Ti
3.33	2.6	0.15	0.12	0.058	0.009	0.009	0.005	<0.1	<0.4	balance

The shielding gas was argon 5.0. The first step of investigation was to evaluate the influence of the vapor plume on the weld pool dynamic. For this purpose it was necessary to record the welding process in slow-motion. During the experiments, a small area of the weld was recorded with two different high-speed cameras, see Figure 2.

Fig. 1. Dimensions of the Ti3Al2.5V workpiece with a thickness of 16 mm.

Both cameras were activated by a trigger signal and could thus be started at the same time. This type of control yielded two synchronously running shots. The first HS camera type FASTCAM-X 1024 PCI captured color images of the plume. The lighting was done by a 700 W lamp (Lichttechnik Typ SW-700 W). The second type HS camera Photron SA 5, took monochrome images of the molten pool and was illuminated by a diode laser (Dilas Compact, 100 W, 808 nm). Both cameras (including the lighting units) and the weld sample itself remained stationary, only the laser beam optics was linearly moved in the welding direction. The laser beam went through the exposure areas of the cameras approximately in the weld center. The recording window of the camera for the plume was about 15 mm wide.

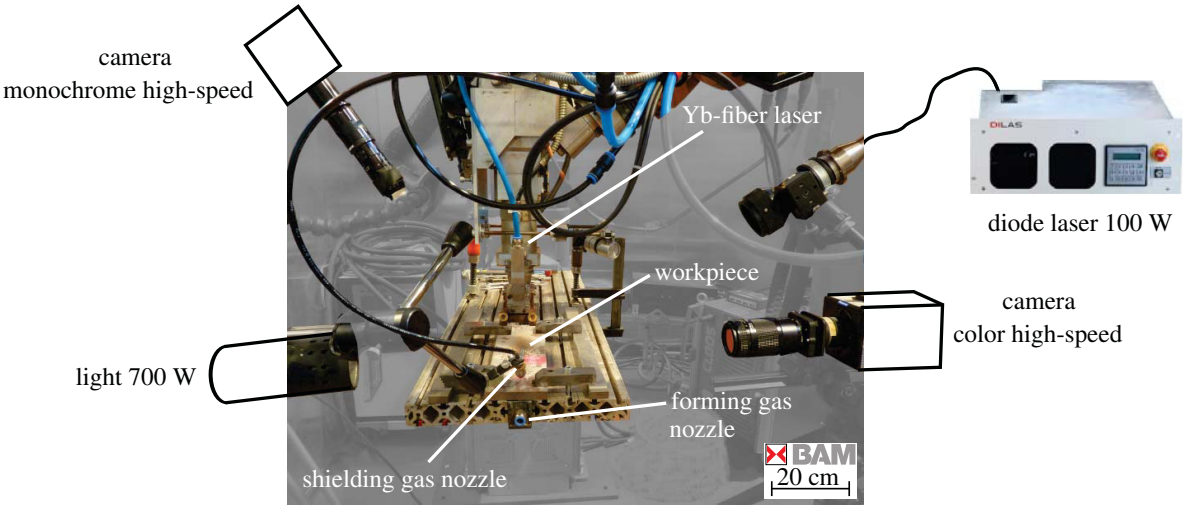

Fig. 2. Experimental setup with two high-speed cameras.

3.1. Low inert gas flow (10 l/min)

In these experiments, the argon shielding gas provided by a laterally arranged nozzle with a flow rate of 10 l/min was applied to the workpiece surface. A trailing ceramic tube with a circular opening 10 mm in diameter was mounted in front of the laser beam in welding direction. A box-shaped forming gas nozzle positioned on the workpiece bottom was also charged with argon inert gas, see Figure 2. A certain amount of shielding gas was required since otherwise no stable welding process would have been achieved. The laser output power was 17.6 kW the welding speed was 1.8 m/min and the laser beam focus distance was located 8 mm under the workpiece surface. In the welding tests with

very little inert gas a significant plume formation was observed. The high-speed images (Figure 3) reveal an unstable welding process over the entire recording area that is associated with a particularly large plume. The weld pool dynamics was characterized by periodical eruptions of the metal droplets which could be attributed to a significant intensifying of the plume in its length and brightness (Figure 3, 10 ms). Therefore the laser beam power transmitted through the plume entering the keyhole results in the decrease of the emerging amount of metal vapor. Simulteneously, the stability of the keyhole surface decreases as result of reduced vapour recoil pressure, which lead to formation and detachment of the liquid dropplet. As the vapor plume ejection becames smaller, the absorbed part of the laser beam power reduces, see picture at the time 15 ms (Figure 3). More laser beam power reaches the keyhole, where it meets the liquid material. Due to the abrupt rise of the laser beam power in the weld pool, a pulse is created which can increase the weld pool dynamic strongly. This results in eruptions of liquid metal, see pictures at the time 23 ms to 29 ms (Figure 3). Quantitative analysis of the individual images have resulted in plume heights of 10 mm to 30 mm.

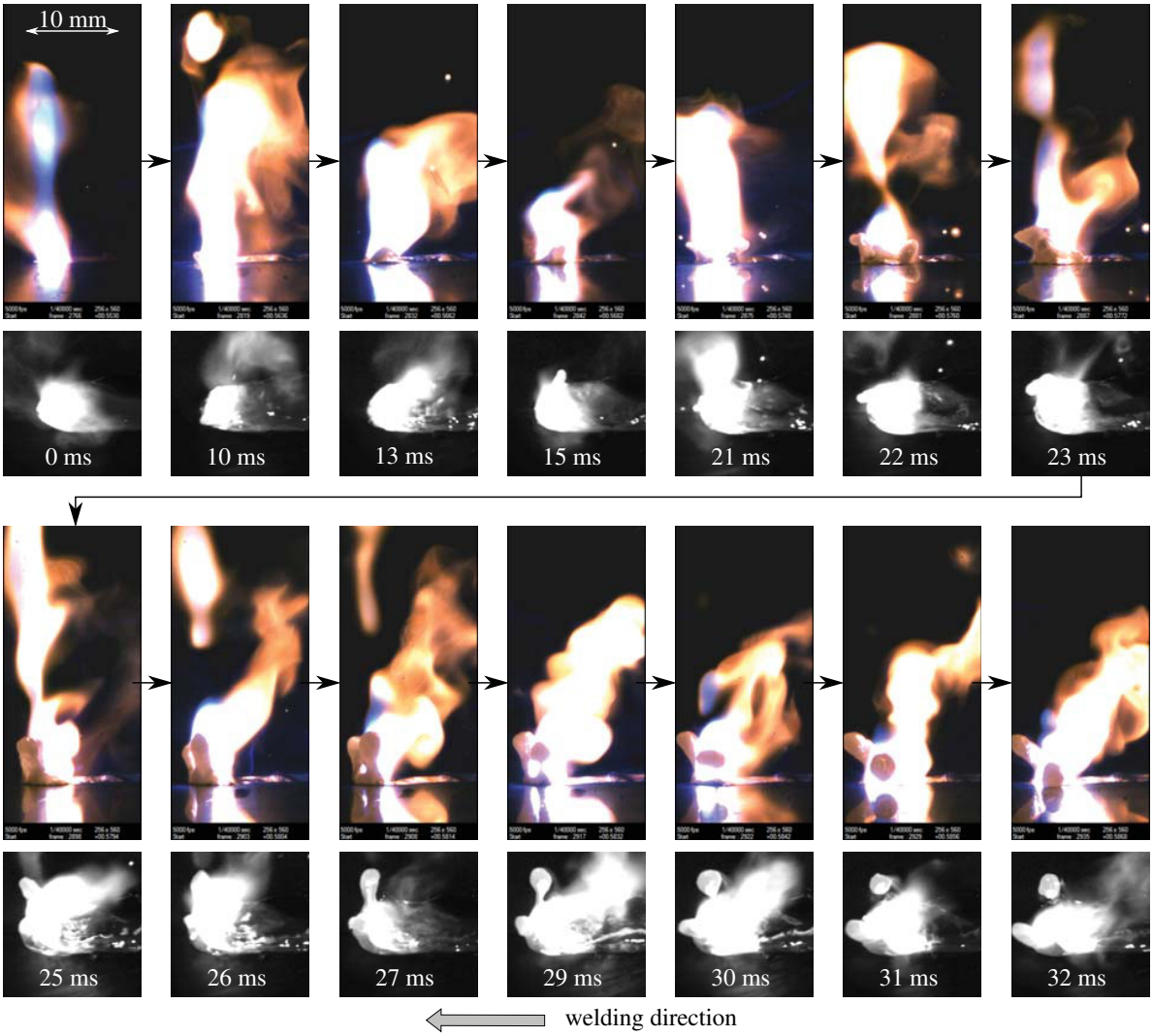

Fig. 3. High-speed image of the welding test with 10 l/min inert gas. Welding parameters: laser power 17.6 kW, focus -8 mm, welding speed 1.8 m/min, shielding gas Argon. Top: vapor plume. Bottom: weld pool.

Similar to the case of high power laser keyhole welding of structural steels (Shcheglov (2012)) the plume can be divided in two zones: the light intensive plasma plume attached to the workpiece surface, and a fume-like cloud of condenced vapour, having a much lower degree of intensity adjacent to this. In places, it is clearly seen how the laser beam couples into this cloud, first picture (Figure 4) at the time 0 ms. In the following pictures it could be seen, as the plasma plume grows and starts to propagate toward the beam direction (0.2 ms to 1.2 ms). Subsequently, the interaction in the vapor plume increases and a part of the laser beam is absorbed which is manifested in increasing of the width and the intensity of the plasma plume, (1.4 ms to 1.8 ms). In the next phase the part of the plasma plume becomes detached from the adjacent to the keyhole part and disappears continuously until the initial situation nearly repeats (2.0 ms to 2.6 ms). The whole cycle of plume evolution takes approximately 3 ms, which fairly good correlates with reported earlier dynamics of the plasma pume with characteristical frequencies of 2 kHz to 3 kHz in case of steel welding (Shcheglov et al. (2011)).

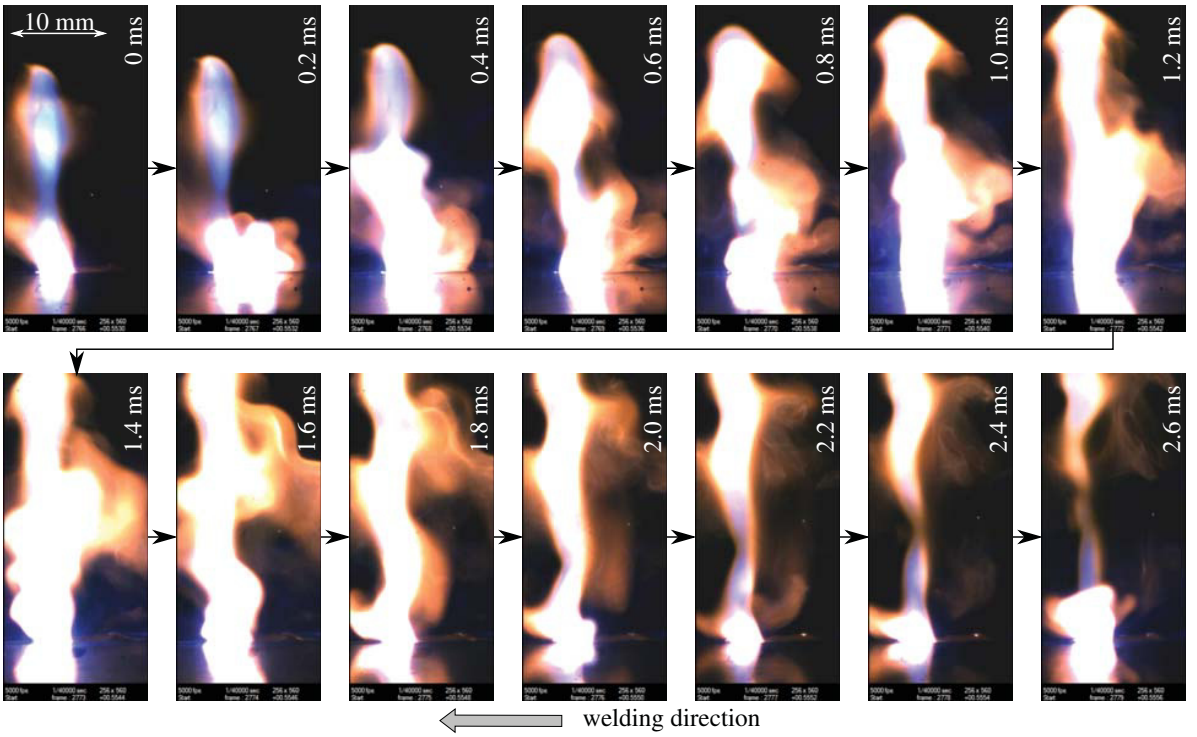

Fig. 4. High-speed image of the vapor plume. Welding parameters: laser power 17.6 kW, focus -8 mm, welding speed 1.8 m/min, Argon 10 l/min.

3.2. Higher inert gas flow (50 l/min)

The same arrangement as under a), with a 5 times higher flow rate of the argon inert gas, i.e. 50 l/min, from the laterally mounted ceramic tube. Increasing the flow rate of the argon inert gas results in a reduction of the exiting plume, see Figure 5. The dynamics in the melt had decreased, the welding process has become much more stable compared to the previous case. In the high-speed image analyses an average plume height of 5 mm to 10 mm could still be detected.

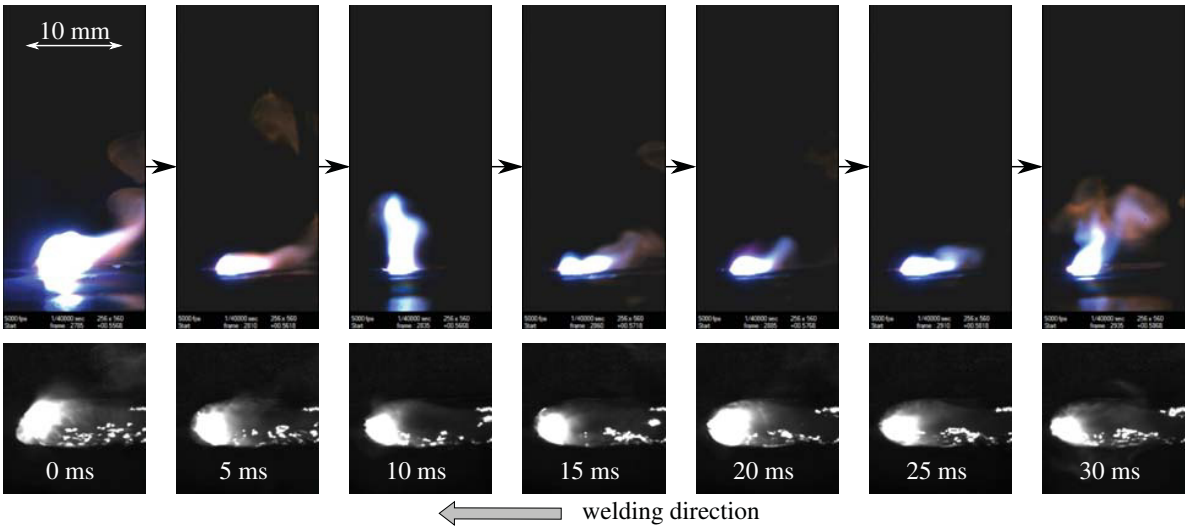

Fig. 5. High-speed image of the welding test with 50 l/min inert gas. Welding parameters: laser power 17.6 kW, focus -8 mm, welding speed 1.8 m/min, shielding gas Argon. Top: vapor plume. Bottom: weld pool.

4. Suppression of the vapor plume by use of a trailing nozzle

A specially designed gas shielding nozzle fulfilled two requirements. Firstly, suppression of the plume by the gas nozzle laterally attached in relation to the welding direction. Secondly, protection of the weld metal from atmospheric gases. The required length of the trailing gas nozzle was determined by measurements of the temperature curve during the cooling process. With the aid of Ni-CrNi-thermocouples temperature measurements were made at two points along the weld. The thermocouples were positioned at a distance of 30 mm from each other and at a distance of 2 mm from the weld center. The results of the temperature measurements are plotted in the diagram in Figure 6. After a cooling time of 5 s or 10 s, the critical temperatures of 400 °C (critical 1) and 300 °C (critical 2) were reached, see Figure 6. Up to the critical temperature 1 the receptivity for atmospheric gases is very high and decreases to the critical temperature 2.

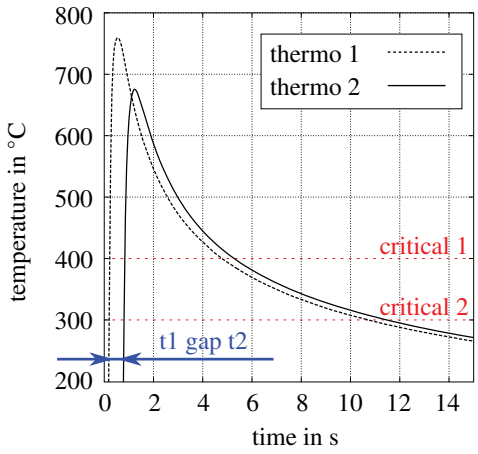

Fig. 6. Measurement of the thermocouples.

Trailing nozzle lengths of 250 mm and 500 mm can be determined. Because the 500 mm trailing nozzle would exceed the sample length and thus no adequate gas shield could be ensured, this variant was discarded. Furthermore, for the 500 mm version of a lower critical temperature of 300 °C was assumed at which the effects of atmospheric gases are significantly lower than at 400 °C. Therefore, only the 250 mm trailing nozzle was used, see Figure 7.

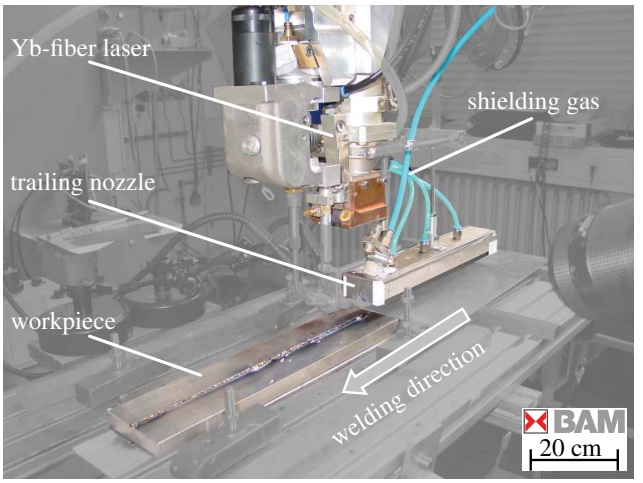

Fig. 7. Experimental setup with trailing nozzle.

5. Results and Discussion

The images of the high speed camera (Figure 3 to 5) show the two different parts of the plume. As it was studied previously for the case of the laser beam welding of steel (Shcheglov (2012)), the temperature of the upper part corresponds approximately to the boiling point and the temperature gradient in this part is small. Thus, the main mechanism of defocusing is the scattering of the laser radiation by condensed particles. As the height of the plume changes randomly, the laser radiation intensity becomes irregular. In the lower part of the plume, having a significant higher temperature with a steeper radial gradient than the upper part, the mechanism of the laser beam defocusing is mainly due to the refraction of the laser radiation on the radial density distribution of the weakly ionized metal vapour jet. The superposition of all these effects results in a dynamically unstable and irregular distributed intensity of the laser radiation at the workpiece surface. The irregular laser power distribution generates strong dynamics in the weld pool. When the frequency of the disturbed laser radiation modulated by the plume behaviour is similar to the eigenfrequency of the weld pool dynamics, a constructive interference occurs and the amplitudes rise. Therefore, the weld pool dynamics are strongly increased and this results in an eruption of liquid metal. The two effects of the specially designed trailing nozzle can be seen in the destructive and nondestructive test results. Preventing the plume formation led to a very stable welding process without significant expel of material. Weld metal porosity was thus reduced, which can well be seen on the radiographs, Figure 8. Since virtually no temper colors could be identified any more neither on the top nor on the bottom side, the oxygen content can be presumed to be less than 0.1 % (Bergmann (2004); Li et al. (2005)). Any temper colors did not occur in both the weld metal and the HAZ area. Hardness measurements in the weld transverse section show no appreciable increase in HAZ hardness, Figure 9 left. The base material hardness was between 240 HV1 and 270 HV1, the measured hardness in the weld metal was between 290 HV1 and 315 HV1. Table 2 shows that the base material samples have a similar yield strength ($R_{p0.2}$), tensile strength (R_m) and strain at failure (A) like the welded samples. As part of the Charpy impact tests (C.i.t.) six welded samples were prepared in accordance with DIN EN 10045. Three of these samples were taken for testing at room temperature and another three samples for testing at 0 °C. In this field of application the surrounding medium is sea water. Thus the minimum temperature for the Charpy test was 0 °C. The results of the tests are shown in Table 2.

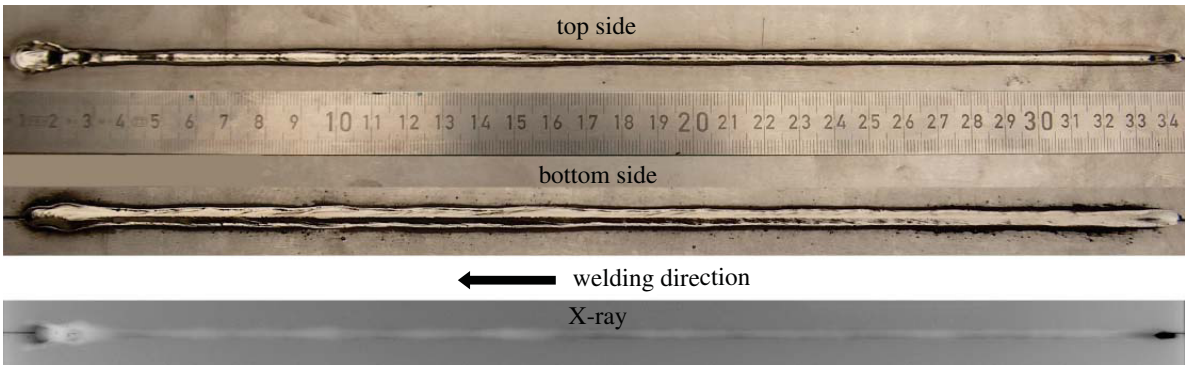

Fig. 8. Trailing nozzle weldseam and X-ray. Welding parameters: laser power 19 kW, focus -8 mm, welding speed 1.8 m/min, shielding gas Argon.

Table 2. Measured stress (R) and strain at failure (A) of the welding with trailing nozzle, C.i.t. = Charpy impact test.

	$R_{p0.2}$ in MPa	R_m in MPa	A in %	C.i.t. at RT in J	C.i.t at 0 °C in J
base metal	660 ± 10	676 ± 13	19 ± 2,0	73 ± 23	
weld metal	645 ± 7	651 ± 5	16 ± 1,1	82 ± 19	89 ± 23

The results reveal nearly idendical values at room temperature and at 0 °C. This is to say that the decrease in temperature in this region has hardly any effect on the ductility of the titanium alloy. Furthermore, all the fracture surfaces exhibit a mixed mode brittle and ductile fracture. Prepared macrosections (Figure 9) show no pores or inclusions, confirming the X-ray image (Figure 8). The other welds in this investigation a small amount pores and achieve the evaluation group B according to DIN EN 13919-1 and EN ISO 5817. The weld surface displays slight concavity, with minor notches at the weld root. Also, slight melt sagging is observed on the weld root. Both imperfections are still within the tolerance range of evaluation group B. The microsections in Figure 9 show a martensitic microstructure in the region of the weld metal.

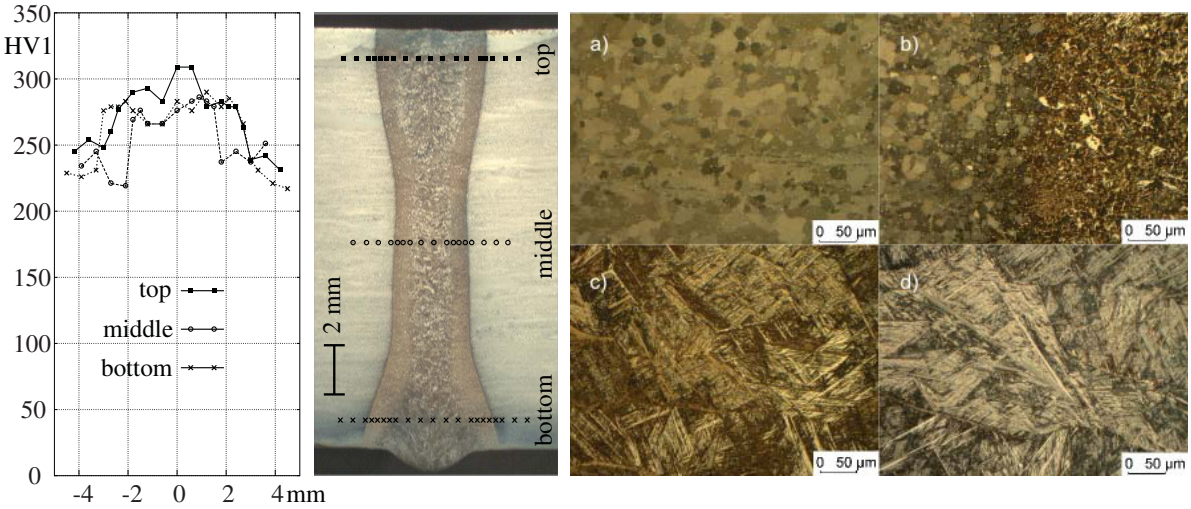

Fig. 9. Welding with trailing nozzle with Argon 5.0. Left: macrosection with the hardness in the top, middle and bottom of the weld seam. Right: microsections of a) base material, b) HAZ, c) and d) weld seam. Welding parameters: laser power 19 kW, focus -8 mm, welding speed 1.8 m/min.

6. Conclusions

At first, it can be stated that a plume on the workpiece surface can adversely affect the welding process during laser beam welding of Ti3Al2.5V. The absorbed portion of the laser beam power in the plume increases with increasing plume size and reduces the energy coupling into the workpiece. The application of a suitable inert gas shield can prevent the plume formation and thus reduce the weld pool dynamics. In addition, the weld metal can effectively be shielded from the influence of the atmospheric gases when using a trailing nozzle. Measured mechanical-technological properties show hardly increase in hardness in the weld metal area. Furthermore, the fracture strain of the weld zone is similarly compared to that of the base material. Charpy impact tests demonstrate that a reduction in temperature from room temperature to 0 °C has no effect on the ductility of the welded material. All samples show approximately equal impact energy and all fracture surfaces feature a mixed mode brittle and ductile fracture. It can be stated in conclusion that butt welding of 16 mm thick Ti3Al2.5V plates using a 20 kW fiber laser is possible when the plume formation is carefully avoided. Moreover, the weld metal shall be shielded during the cooling phase from the influence of the atmospheric gases. The results in this investigations with the trailing nozzle show satisfactorily welding seams.

Acknowledgements

The authors are grateful to ThyssenKrupp Marine Systems GmbH for their support.

References

Anisimov, S., 1967. Impact of high power radiation on metals. National Technical Information Service.

Bergmann, J., 2004. Influence of the oxygen content in the shielding gas on microstructure and machanical properties of laser welds of titanium alloys. Materialwissenschaften und Werkstofftechnik 35(9), 543–556.

Boyer, R., Welsch, G., Collings, E., 2007. Materials Properties Handbook: Titanium Alloys. ASM - International, The Materials Information Society.

Bungardt, K., Rüdinger, K., 1956. Beitrag zur Frage des Schweissens von Titan und Titanlegierungen. Zeitschrift für Metallkunde 47, 585–593.

Caplan, I.L., 1986. Ti-3Al-2.5V for Seawater Piping Applications. ASTM International - Industrial Applications of Titanium and Zirconium , 43–53.

DVS2713, 2003. Schweissen von Titanwerkstoffen, Werkstoffe - Prozesse - Fertigung - Prüfung und Bewertung von Schweissverbindungen. DVS - Deutscher Verband für Schweissen und Verwandte Verfahren e.V.

Hügel, H., Dausinger, F., 2004. Laser Applications. Springer-Verlag.

Li, R., Li, Z., Zhu, Y., Rong, L., 2010. A comparative study of laser beam welding and laser MIG hybrid welding of TiAlZrFe titanium alloy. Materials Science and Engineering A 528, 1138–1142.

Li, X., Xie, J., Zhou, Y., 2005. Effects of oxygen contamination in the argon shielding gas in laser welding of commercially pure titanium thin sheet. Journal of Materials Science 40, 3437–3443.

Malletschek, A., 2011. Einfluss von Titan auf den Entwurf von Unterwasserfahrzeugen. Ph.D. thesis. TUHH - Technische Universtät Hamburg-Harburg.

Peters, M., Leyens, C., 2002. Titan und Titanlegierungen. Wiley-VCH.

Shcheglov, P., 2012. Study of Vapor-Plasma Plume during High Power Fiber Laser Beam Influence on Metals. Ph.D. thesis.

Shcheglov, P., Uspenskiy, S., Gumenyuk, A., Petrovskiy, V., Rethmeier, M., Yermachenko, V., 2011. Plume attenuation of laser radiation during high power fiber laser welding. Laser Physics Letters 8, 475–480.

Tu, J.F., Inoue, T., Miyamato, I., 2003. Quantitative characterization of keyhole absorption mechanisms in 20-kW-class-CO2 laser welding process. Journal of Physics: Applied Physics 36, 192–203.

Yi, Z., Li, L., Zhang, G., 2005. Spectroscopic measurement of plasma inside the keyhole in deep penetration laser welding. Journal of Physics: Applied Physics 38, 703–710.